Numerical Simulation of Non-Newtonian Fluid Flow across a Sinusoidal Microchannel

Pranay Kumar Pandey[1]

[1]Dept. of Aerospace Engineering, Amity University Mumbai, Panvel, Maharashtra 410206

Mentor: Binayak Lohani[2]

[2]FOSSEE, IIT Bombay, Mumbai, Maharashtra 400076, India

Supervisor: Prof. P. R. Naren[3]

[3]School of Chemical & Biotechnology, SASTRA Deemed to be University, Tamil Nadu 613004

Abstract

Flow of non-Newtonian fluids through sinusoidal microchannels is studied in the current work. The work aims to simulate different flow features such as velocity profile, pressure gradient, viscosity profile in flow of non-Newtonian fluid through a sinusoidal microchannel. The work is motivated by the growing interest in designing efficient microfluidic devices that can handle complex fluids, such as biological fluids, polymer solutions, and suspensions (Nguyen & Nguyen, 2012). Understanding the flow characteristics of such fluids in microchannels provides valuable insights into optimizing microchannel design for specific applications. The geometry under consideration is adopted based on Mondal et al. 2019 (Figure 1) and the fluid system used for the simulation study are presented in Table 1

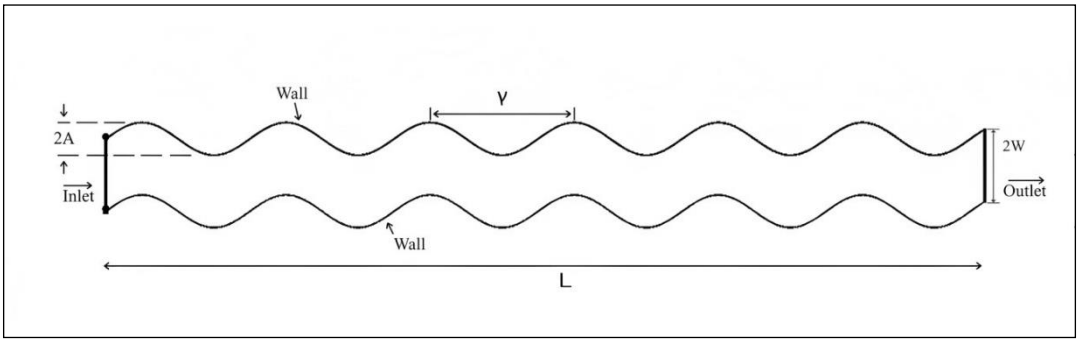

Figure 1: Schematic Sketch of the geometry

Table 1: Details of non-Newtonian Fluids

Fluid	**Density (kg/m^3)**	**K (Pa.s^n)**	**n (-)**
Blood	1060	0.004	0.90
Cellulose	1006	0.025	0.82
Xanthan Gum	1143	0.55	0.39
Crude Oil	970	2.8811	0.9305
Printer Ink	1220	3.783	0.7925

References

Mondal, B., Mehta, S.K., Patowari, P.K. and Pati, S. (2019). Numerical study of mixing in wavy micromixers: comparison between raccoon and serpentine mixer. *Chemical Engineering and Processing - Process Intensification*, 136, 44–61.

Nguyen Q-H and Nguye N-D (2012) Incompressible Non-Newtonian Fluid Flows. In *Continuum Mechanics - Progress in Fundamentals and Engineering Applications*, Eds. Gan Y. X., 47 - 71

Contents

1. Introduction

Microchannels are of paramount importance in diverse applications, particularly in the realm of microfluidics, where they enable precise manipulation and control of minute fluid volumes. Westermaier and Kowalczyk 2020 studied different non-Newtonian fluids, highlighting the numerical results of the test cases. It was revealed that the usage of liquids with different viscosity characteristics leads to significant changes in the behaviour of the compressible two-phase flow. Given the prevalence of non-newtonian behaviour in biological and complex fluids like polymer melts, and foodstuffs like cream and ketchups, encountered in industrial processes, a comprehensive understanding of the flow dynamics of such fluids within microchannels becomes imperative.

The knowledge of microfluidics bears significant implications for optimizing the performance and reliability of microfluidic devices leading to tailored drug delivery systems that capitalize on the unique rheological properties of non-Newtonian fluids. Furthermore, this research can extend its impact to the domain of chemical engineering, where microreactors play a pivotal role in optimizing chemical processes. Edward et al. 1972 developed an explicit finite difference technique which gives instantaneous velocities with an accuracy better than 1 per cent for unsteady, laminar flows of power law liquids in pipes. In the field of biomedicine, these microfluidic devices find utility in drug delivery, diagnostic testing, and cell analysis, offering notable advantages such as reduced sample consumption, accelerated reaction times, and superior fluid flow management.

Craven et al. 2022 presented a Poisson equation method for prescribing fully developed inlet conditions for the flow of either Newtonian or non-Newtonian fluids in CFD models of arbitrary cross-section. The method is shown to be far superior to alternative approaches for prescribing fully developed inlet conditions in such complicated geometries. Gorthi et al. 2020 experimentally investigated capillary filling characteristics of inelastic non-Newtonian fluids in the regime compatible with a zone with balanced capillary and viscous forces using Shear-Thinning Non-Newtonian Fluid.

By investigating the behaviour of non-Newtonian fluids within microreactors, researchers can unlock opportunities for enhanced mixing efficiency, improved reaction kinetics, and superior product quality, streamlining pharmaceutical and chemical manufacturing processes. The profound implications of microchannels in microfluidics and microreactors, coupled with the intrinsic complexities of non-Newtonian fluids, underscore the significance of this research,

poised to catalyse groundbreaking advancements with transformative implications for diverse industries.

Table 2: Details of non-Newtonian Fluid

Fluid	**Density (kg/m^3)**	**K (Pa.s^n)**	**n (-)**
Blood [Nguyen & Nguyen, 2012]	1060	0.004	0.90
Cellulose [Gorthi et al. 2020]	1006	0.025	0.82
Xanthan Gum [Roumpea et al. 2017]	1143	0.55	0.39
Crude Oil [Sami et al. 2017]	970	2.8811	0.9305
Printer Ink [Peng et al. 2021]	1220	3.783	0.7925

- **Blood** is a biological fluid present in living beings and among the most common Non-Newtonian fluid encountered in day-to-day life.
- **Cellulose** is a biopolymer.
- **Xanthan Gum** is used as a food additive as a thickening and emulsifying agent.
- **Crude Oil** is the source of fuel such as petrol, diesel and kerosene.
- **Printer Ink** is made up of Polyacrylamide (PAM) which is also useful in the paper and print industry.

All the above fluid follows the power-law model of viscosity of fluid. Based on the literature studies, it became eminent to carry out analysis with fluids obeying Power-law model. Almost every non-Newtonian fluid can be modelled using this model due to its simplicity and wide availability of experimental dataset and values of its parameters of the governing equation.

2. Literature Review

The provided table offers an overview of a selection of undertakings centred around non-Newtonian fluids. It notably encapsulates a compilation of numerical investigations, the details of which are briefly delineated within Table 2.

Table 2 : Literature Study

Type of Study	Numerical	Numerical	Numerical	Numerical					Numerical	Numerical
Reference	Edwards et al. 1972	Philippou et al. 2016	Koh et al. 2004	Westermaier and Kowalczyk 2020					Craven et al. 2022	Keslerová 2023
Fluid	Generic	Generic	polyoxymethylene	water	blood	0.1 % xanthan gum solution	activated sludge	ketchup	blood	blood
Viscosity Model	Power Law	Bingham-plastic	Modified Power Law	Bird-Carreau	Cross Power Law	Casson	Herschel and Bulkley	Power-law	Carreau–Yasuda	Newtonian, Carreau and Power Law
Geometry	pipe	tubes and channels	channel	backward-step					arbitary cross section	S-type bypass
Mesh	N/A	32,000	N/A	2,46,800 hexahedral elements					7 million elements	4.2 million tetrahedral elements

3. Geometry

The geometry considered in the current work is adopted based on Mondal et al. 2019. The schematic sketch of the geometry is shows in Figure 2. The sinusoidal component of the microchannel geometry has been represented using the following mathematical expressions.

Top Wall

$$S(x) = L + A\sin\left(\frac{2\pi x}{\gamma}\right)$$

Bottom Wall

$$S(x) = -L + A\sin\left(\frac{2\pi x}{\gamma}\right)$$

Where A denotes the amplitude of the wall surface and γ denotes wavelength of the wall surface. In this current work, we have taken, half-width $W = 150\mu m$, $Dimensionless\ amplitude\ \propto = 0.45$ and $dimensionless\ wavelength\ \lambda = 4$

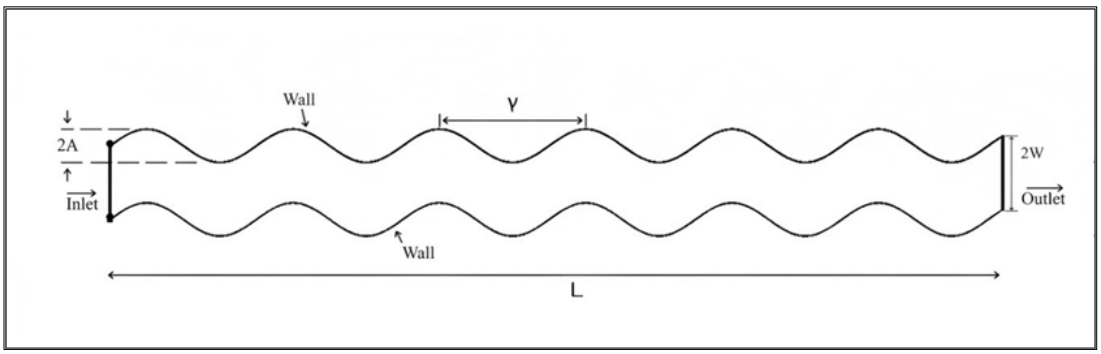

Figure 2 : Schematic sketch of the geometry along with the boundary condition used in the current work

3.1 Mathematical Model

The two-dimensional flow through the sinusoidal microchannel is modelled as steady-incompressible-laminar flow of Non-Newtonian Fluid. The thermophysical properties of the fluids are assumed to be constant. The transport properties are defined as per the data obtained from literature survey. The governing equations of continuity and momentum and mass transfer can be expressed as follow.

Continuity Equation

$$\frac{\partial \mathrm{u}}{\partial \mathrm{x}} + \frac{\partial \mathrm{v}}{\partial \mathrm{y}} = 0$$

x-momentum equation

$$\rho\left(\mathrm{u}\frac{\partial \mathrm{u}}{\partial \mathrm{x}} + \mathrm{v}\frac{\partial \mathrm{u}}{\partial y}\right) = -\frac{\partial p}{\partial x} + \mu_{\mathrm{PL}}\left(\frac{\partial^2 \mathrm{u}}{\partial \mathrm{x}^2} + \frac{\partial^2 \mathrm{u}}{\partial \mathrm{y}^2}\right)$$

y-momentum equation

$$\rho\left(\mathrm{u}\frac{\partial \mathrm{v}}{\partial \mathrm{x}} + \mathrm{v}\frac{\partial \mathrm{v}}{\partial \mathrm{y}}\right) = -\frac{\partial p}{\partial x} + \mu_{\mathrm{PL}}\left(\frac{\partial^2 \mathrm{v}}{\partial \mathrm{x}^2} + \frac{\partial^2 \mathrm{v}}{\partial \mathrm{y}^2}\right)$$

Power-Law model of Viscosity

$$\boldsymbol{\tau = k\left(\frac{\partial u}{\partial y}\right)^{n}}$$

Dividing the above equation with $\left(\frac{\partial \mathrm{u}}{\partial \mathrm{y}}\right)$ we get,

$$\boldsymbol{\mu_{\mathrm{PL}} = k\left(\frac{\partial u}{\partial y}\right)^{n-1}}$$

where,

μ_{PL} is the viscosity of the power law fluid

τ is the shear stress

k is the flow consistency Index $(\mathrm{Pa.s^n})$

$\frac{\partial \mathrm{u}}{\partial y}$ is the shear strain rate also known as velocity profile $(\mathrm{s^{-1}})$

n is the flow behaviour index (-)

Reynolds Number for Newtonian Fluids is described according to equation given below:

$$\mathrm{Re} = \frac{\rho\ \mathrm{v}\ \mathrm{W}}{\mu}$$

Metzner et al. 1955 described Reynolds Number for Power-Law Fluids as below :

$$\mathrm{Re_{PL}} = \frac{\rho\ \mathrm{v}^{2-\mathrm{n}}\ \mathrm{W}^{\mathrm{n}}}{K\left(\frac{3n+1}{4n}\right)^{n} 8^{n-1}}$$

4. Details of Computational Mesh

The mesh consists of 49,765 quadrilateral elements. It was made using Ansys 2023 R1 Student. Inflation layers were added to enhance capturing of flow behaviour near the walls.

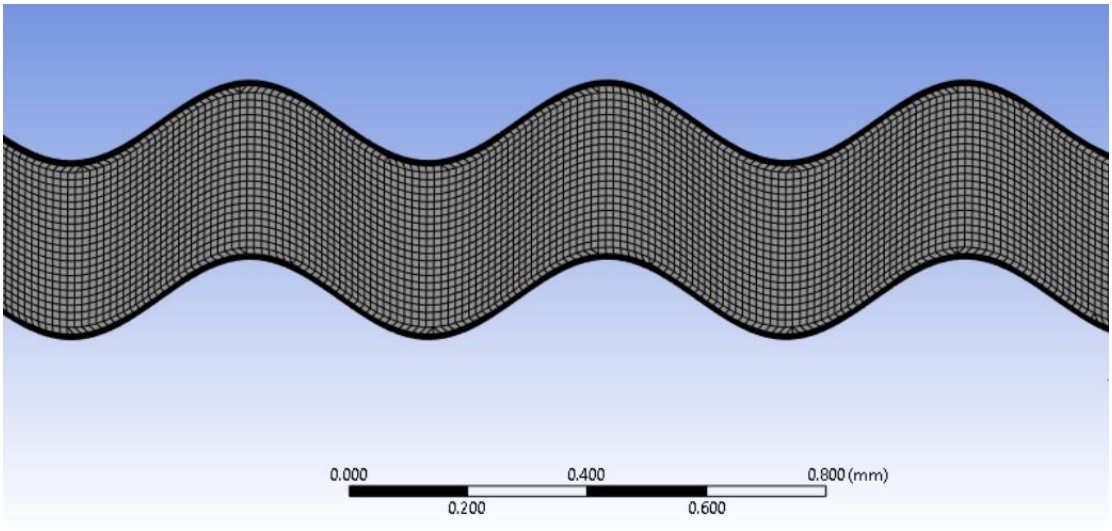

Figure 3a : Representation of Mesh

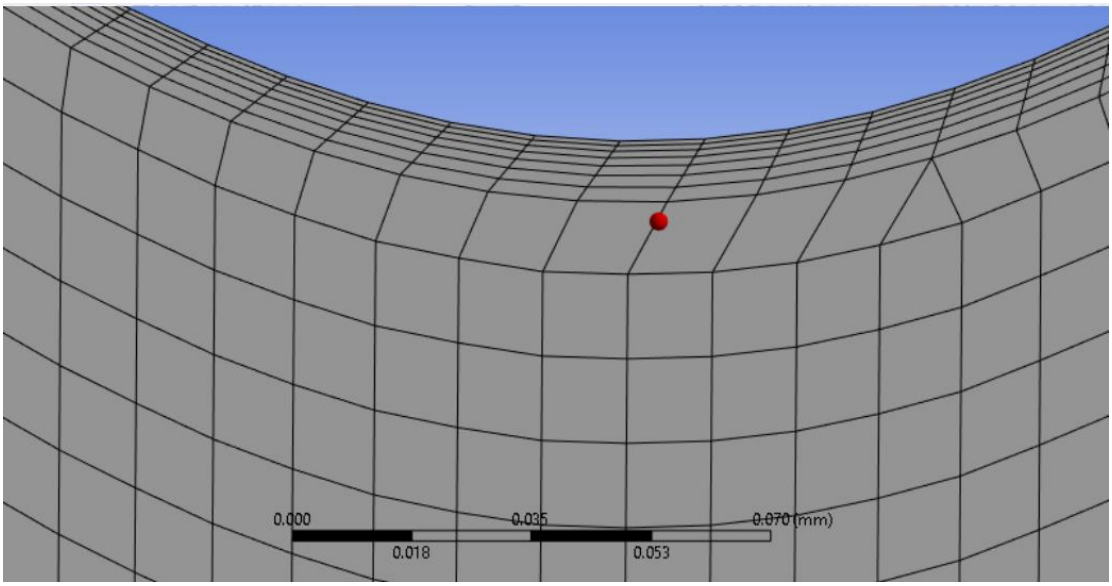

Figure 3b : Close-up view of Inflation Layer

The mesh quality for the mesh used in the simulation has been further presented in Table 3.

Table 3: Mesh Metrics

	Skewness	**Aspect Ratio**
Minimum	0.0005	1.0006
Maximum	0.8013	25.022
Average	0.30805	5.2411
Standard Deviation	0.1088	5.9635

4.1 Boundary Conditions

The simulation was done for a range of velocity between 0.1 m/s and 2.5 m/s. Viscosity model and its' parameters were added in the *transportProperties* file in the *constan*t folder. Properties of Xanthan included in the mentioned file is given below for understanding purposes.

```
rho 1143;
transportModel powerLaw;
powerLawCoeffs
{
  nuMax   [ 0 2 -1 0 0 0 0 ] 1e+01;
  nuMin    [ 0 2 -1 0 0 0 0 ] 1e-05;
  k          [ 0 2 -1 0 0 0 0 ] 0.55;
  n          [ 0 0  0 0 0 0 0 ] 0.39;
}
```

It is important to note that the solver computes kinematic viscosity of the fluid. The details of boundary conditions are given in Table 4.

Table 4: Boundary Conditions of the Setup

Field Variable	**Velocity (U)**	**Pressure (P)**
inlet	fixedValue	zeroGradient
outlet	zeroGradient	zeroGradient
wall	noSlip	zeroGradient

4.2 Solver Setup

The present study was carried out using OpenFOAM v2212 using the simpleFoam solver. The simpleFoam solver in is a steady-state, incompressible flow solver, suitable for simulating laminar and turbulent flows. It employs the ***SIMPLE*** (Semi-Implicit Method for Pressure-Linked Equations) algorithm, a well-established iterative solver widely used in CFD simulations. The SIMPLE algorithm is particularly effective for steady-state problems where time-dependent behaviour is not of interest. By utilizing a segregated approach, the SIMPLE algorithm decouples the velocity and pressure fields, making it computationally efficient and robust for a range of flow conditions.

4.3 Convergence Study

The solution convergence has been inferred from the Residuals plot. Plots of printer ink, water and blood to ascertain it. The variables of 'p' and 'U' are seen to be invariant over a period of time. Depending on the fluid, invariancy occurs early for water which is a Newtonian fluid as denoted in Figure 4b. However, non-Newtonian fluids requires comparatively more iterations to show the invariant nature of variables which has been ascertained in the figures 4a and 4c. However, residual plot for water which is shown in figure 4b, takes relatively less iterations for convergence.

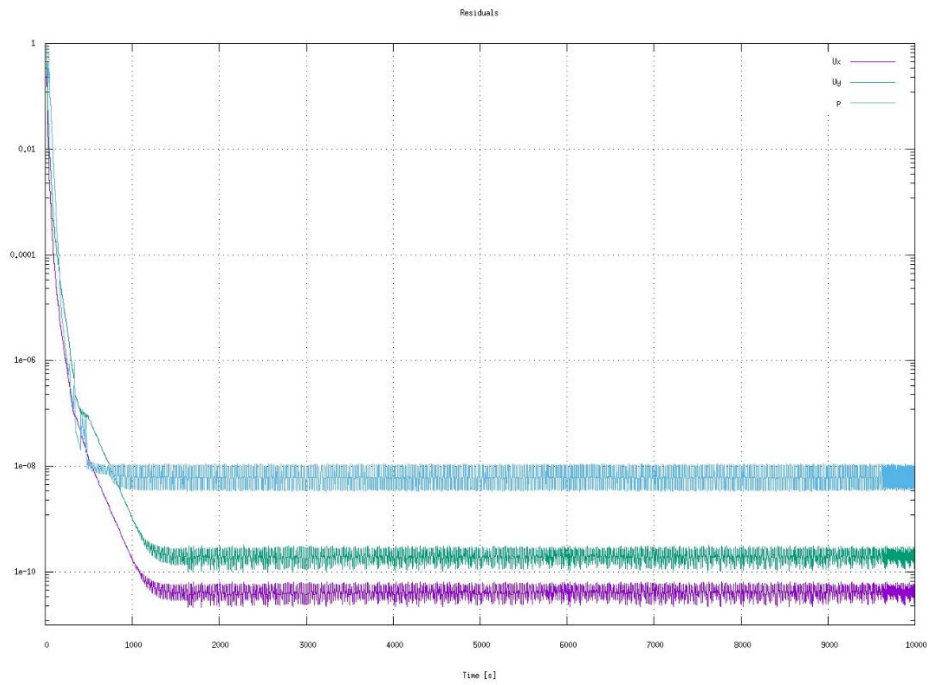

Figure 4a : Residuals plot for blood for velocity = 0.5 m/s

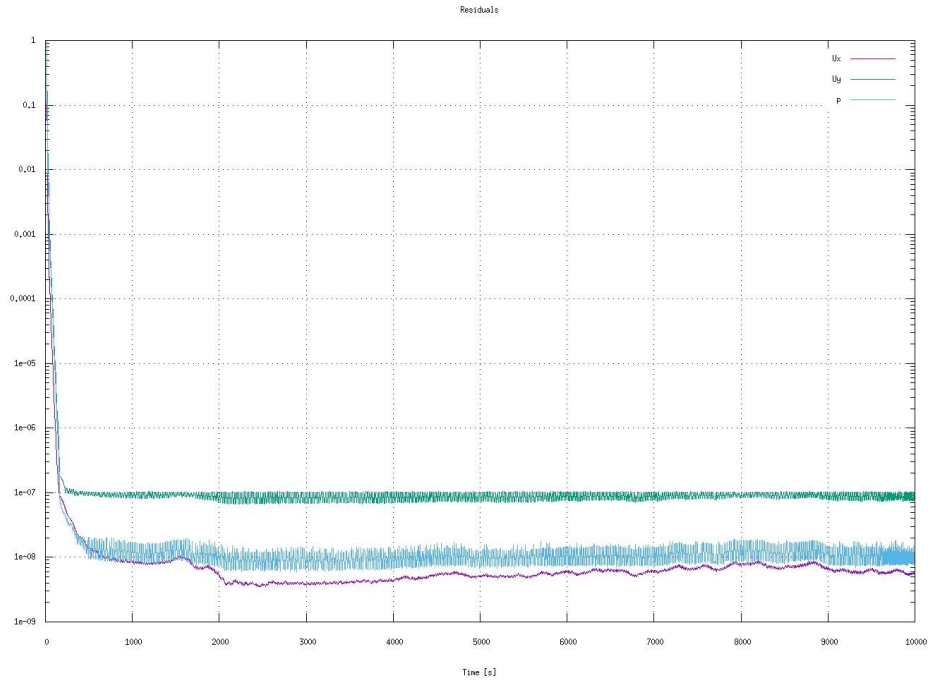

Figure 4b : Residuals plot for water for velocity = 0.5 m/s

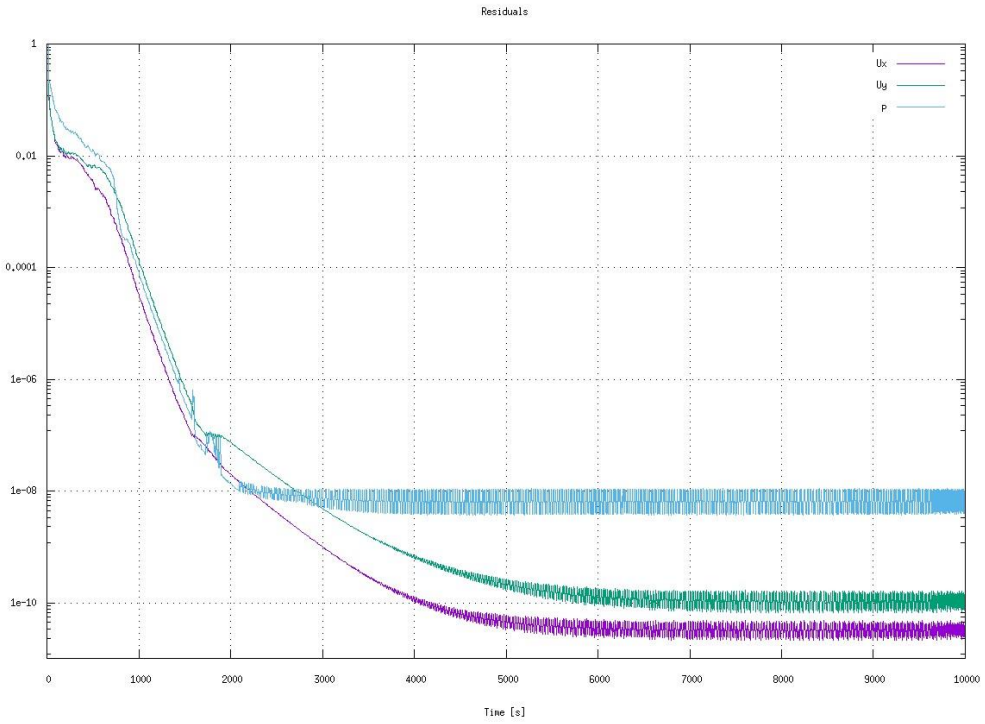

Figure 4c : Residual Plot for xanthan for velocity = 0.5 m/s

5. Figures

To better understand how the simulation appears on reaching end time, figures have been shown. Crude Oil at a velocity of 1 m/s is considered. Velocity profile, pressure variation, distribution of kinematic viscosity and streamline of the flow is presented.

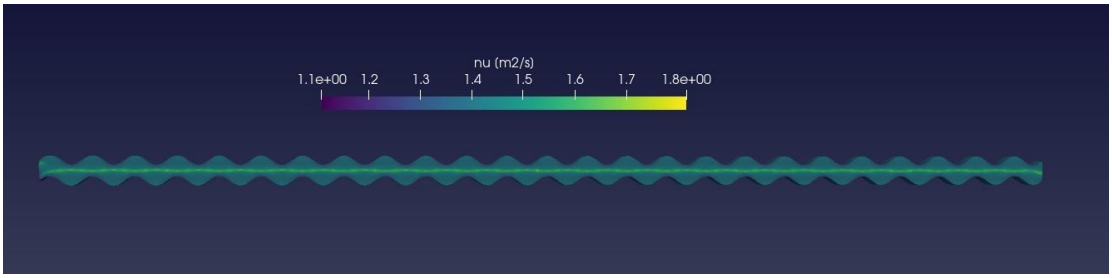

Figure 5a : Kinematic viscosity for crude oil at velocity = 1 m/s

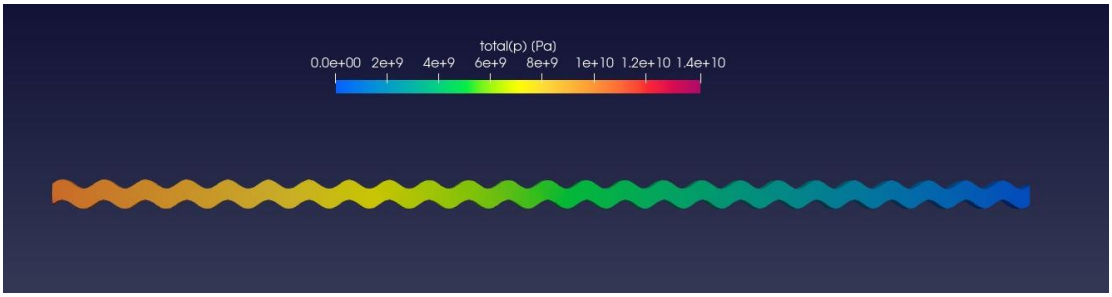

Figure 5b : Total Pressure (Pa) for crude oil at velocity = 1 m/s

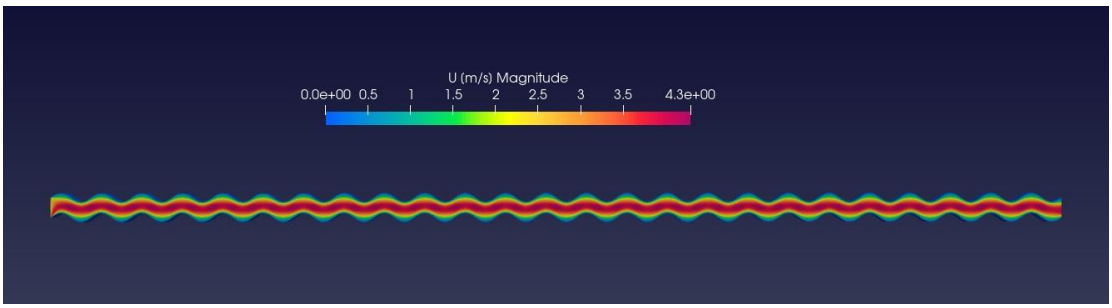

Figure 5c : Velocity (m/s) for crude oil at velocity = 1 m/s

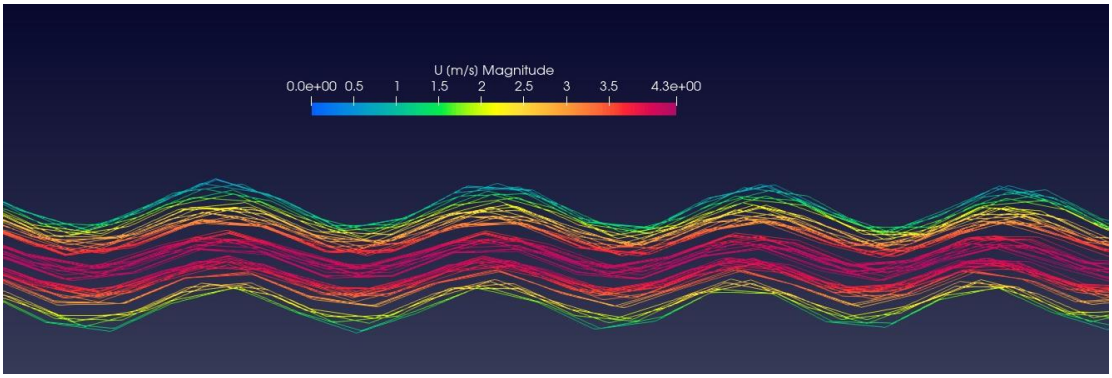

Figure 5d : Velocity streamline for crude oil at velocity = 1 m/s

6. Results & Discussions

The simulation was done for different power-law fluids (as given in Table 1) for a range of inlet superficial velocity from 0.1 to 2.5 m/s. The simulations were converged as described in Section 4.4 The variation of pressure along the length of the channel for different non-newtonian fluids at inlet velocity of 0.1 m/s is shown in Figure 6a and Figure 6b Notably, for flow consistency index K values greater than 1, such as flow of crude oil and printer ink, a considerably higher-pressure variation was noticed, exceeding the order of 10^3, compared to K values less than 1. This pronounced pressure variation can be attributed to the non-linear flow behaviour exhibited by non-Newtonian fluids, following the power-law model in this case.

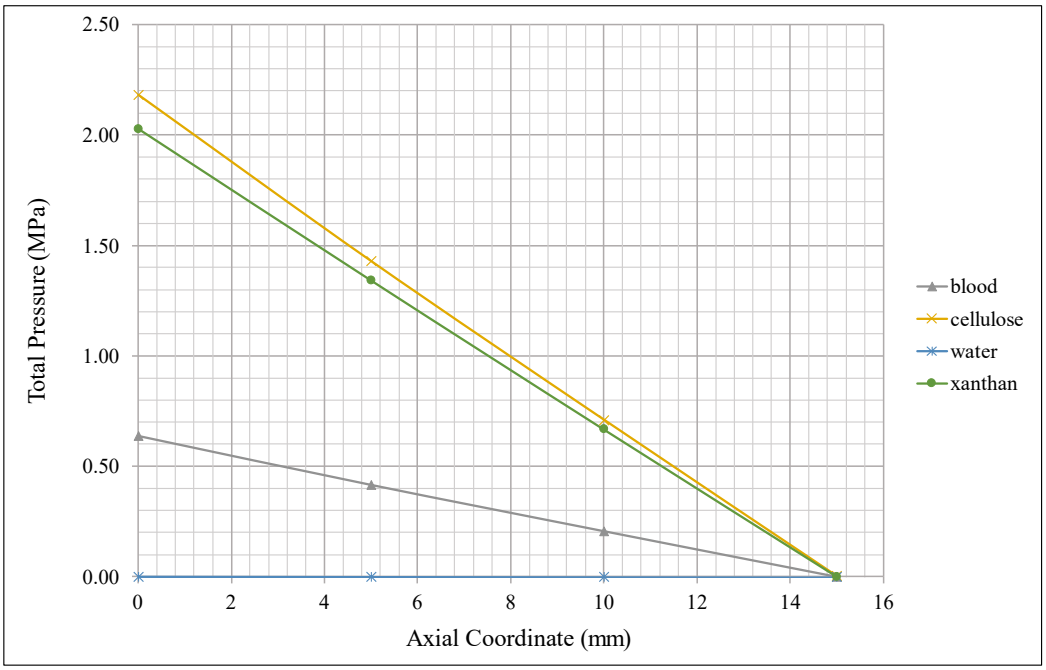

Figure 6a : Total Pressure vs Axial Coordinate for Velocity = 0.1 m/s

Variation of pressure along the length of the channel for water is also shown in Figure 6a for sake of comparison with the behaviour of non-Newtonian fluid. However, unlike non-Newtonian fluids, the pressure variation in water was found to be remarkably low. This behaviour is anticipated, considering Newtonian fluids' constant viscosity regardless of the shear rate, in contrast to the sensitivity of non-Newtonian fluids' viscosity to the applied shear rate. Consequently, the observed minimal pressure gradient variation in water reaffirms its Newtonian nature, further validating the credibility of our simulations.

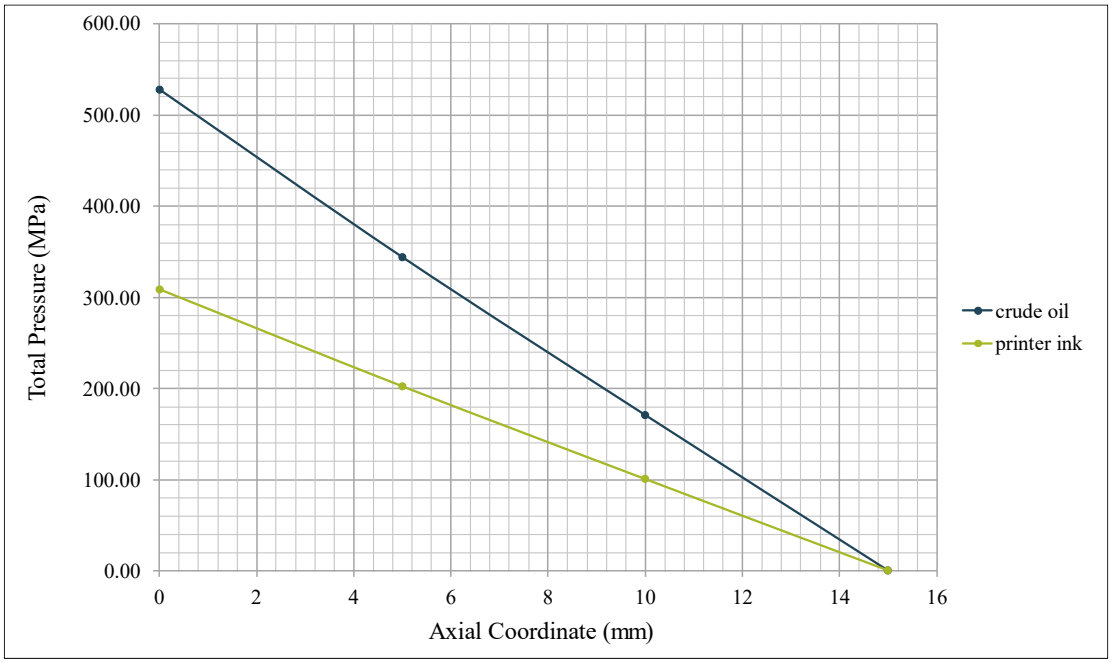

Figure 6b : Total Pressure vs Axial Coordinate for Velocity = 0.1 m/s

The cross-sectional profile of velocity at the outlet boundary is shown in Figure 7. In case of Newtonian fluid, water, the velocity profile at the exit plane, reached its maximum value at a dimensionless width of approximately 0.4. Interestingly, power-law fluids considered for study also demonstrated a similar trend, achieving their maximum velocity at dimensionless width around 0.4. However, the exception to this pattern was observed in the case of Xanthan. The observation of these unique velocity profiles sheds light on the influence of fluid rheology on flow behaviour in complex geometries.

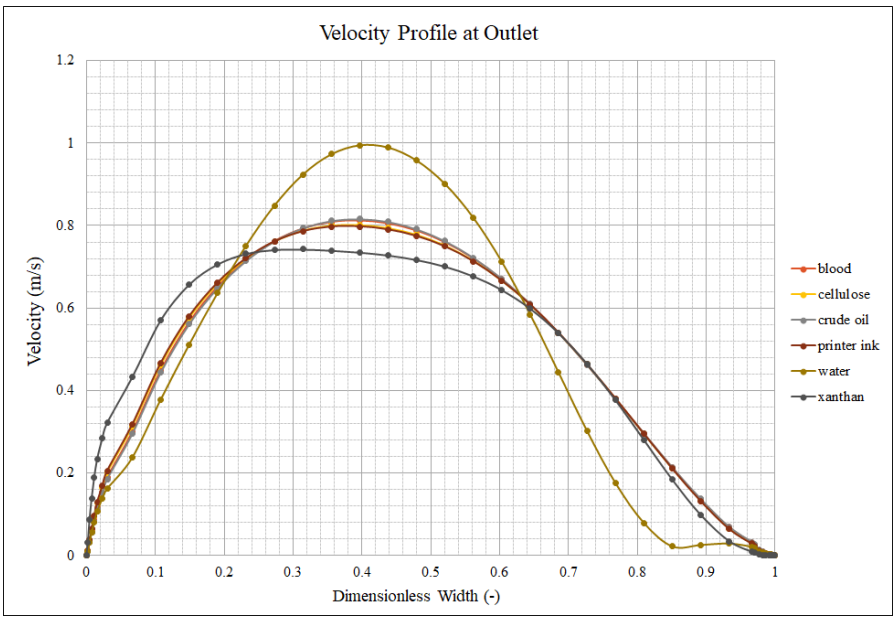

Figure 7 : Velocity Profile at Outlet vs Dimensionless Width for Velocity = 0.5 m/s

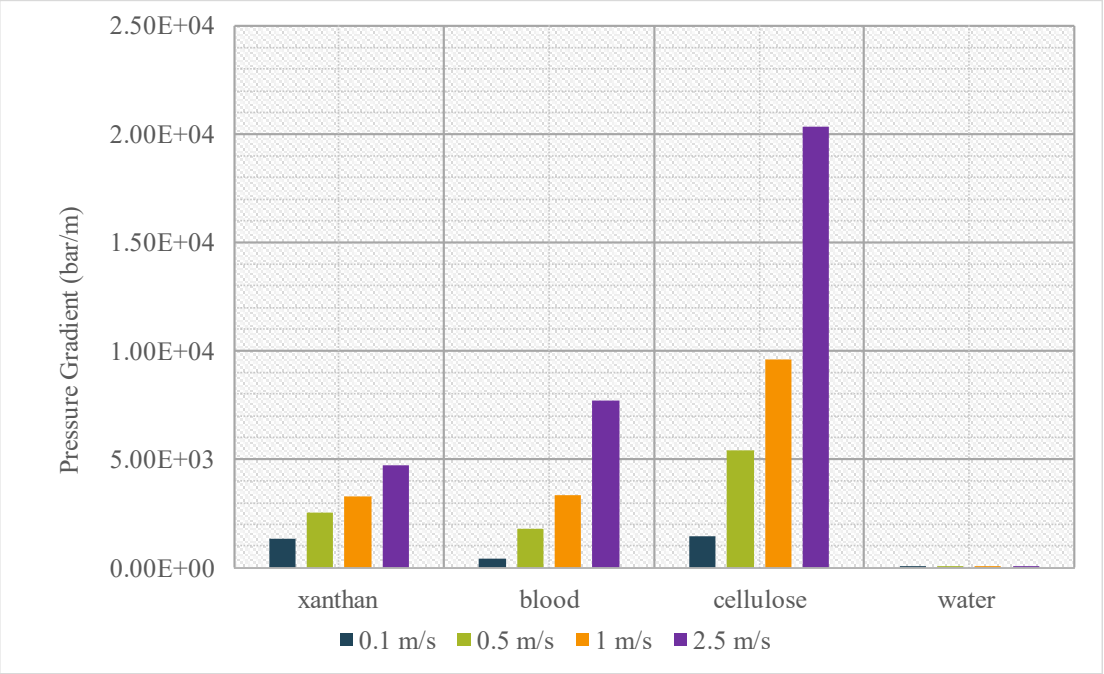

Figure 8a : Pressure Gradient vs Fluid

A direct relationship between fluid velocity and pressure gradient across the total length is shown in Figures 6a and 6b. As the fluid velocity increases, there is a corresponding rise in the pressure gradient along the sinusoidal microchannel. This observation aligns with fundamental fluid mechanics principles, where faster flow velocities generate higher shear rates, resulting in increased frictional forces and pressure drops. The positive correlation between velocity and pressure gradient underscores the significance of variations in flow rates which significantly impact the pressure distribution.

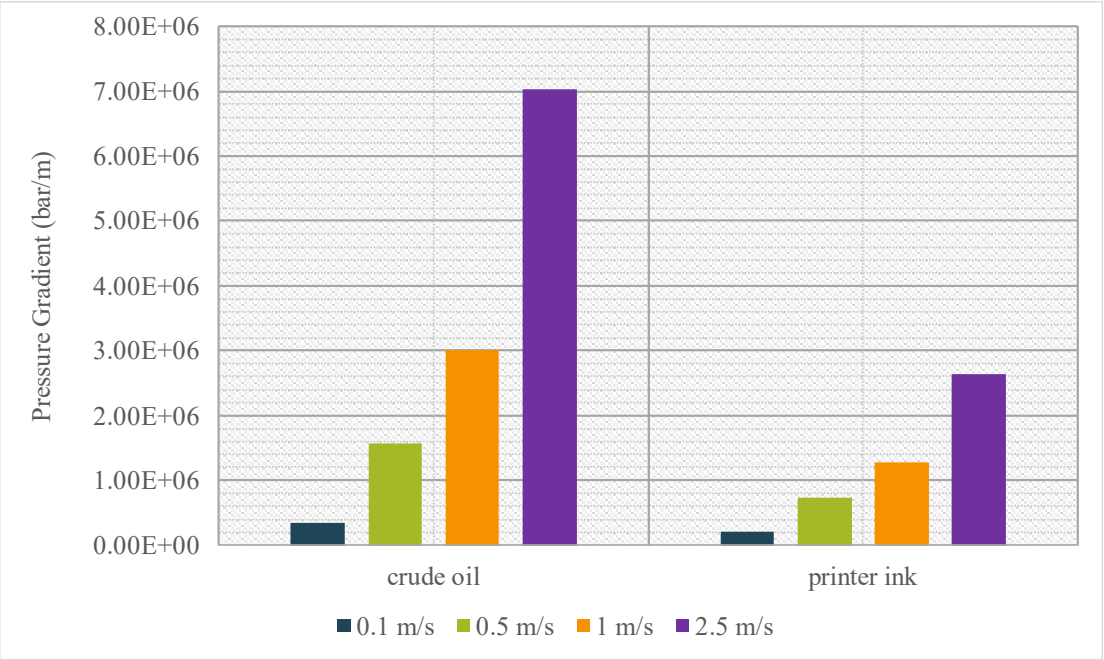

Figure 8b : Pressure Gradient vs Fluid

One significant feature of simulating non-newtonian fluid flow is to observe the variation of kinematic viscosity of the fluid in the flow conditions. In a non-newtonian flow, the kinematic viscosity is affected by the shear stress, thus by the velocity profile. The variation of kinematic viscosity across the channel centre is shown in Figures 9a and 9b. Kinematic viscosity of water (ν) is constant with a value 1e-6 m^2/s. 'ν' shows similar patterns in all the non-Newtonian fluids of being symmetric across the dimensionless width of 0.5. There is a rapid increase in the value of kinematic viscosity between dimensionless width of 0.4 and 0.5 of the channel cross section. In the similar fashion a rapid fall in the values of kinematic viscosity after reaching peak at around 0.5 observed. The observations have indicated that the kinematic viscosity is affected by 'K'.

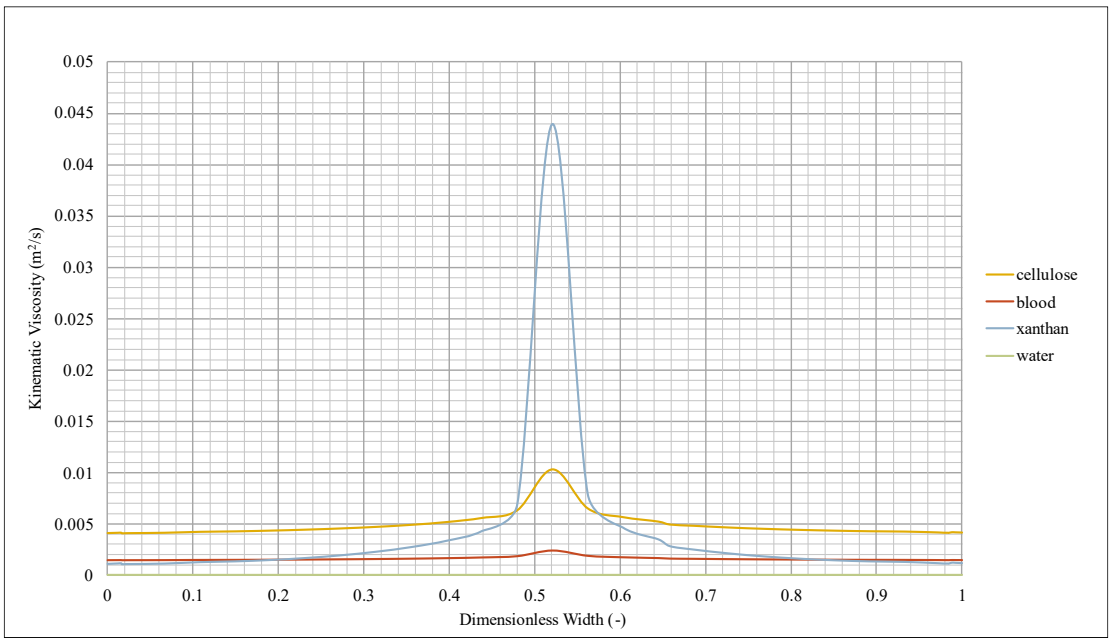

Figure 9a : Kinematic Viscosity at 'x = 7.5 mm' vs Dimensionless Width for Velocity = 0.5 m/s

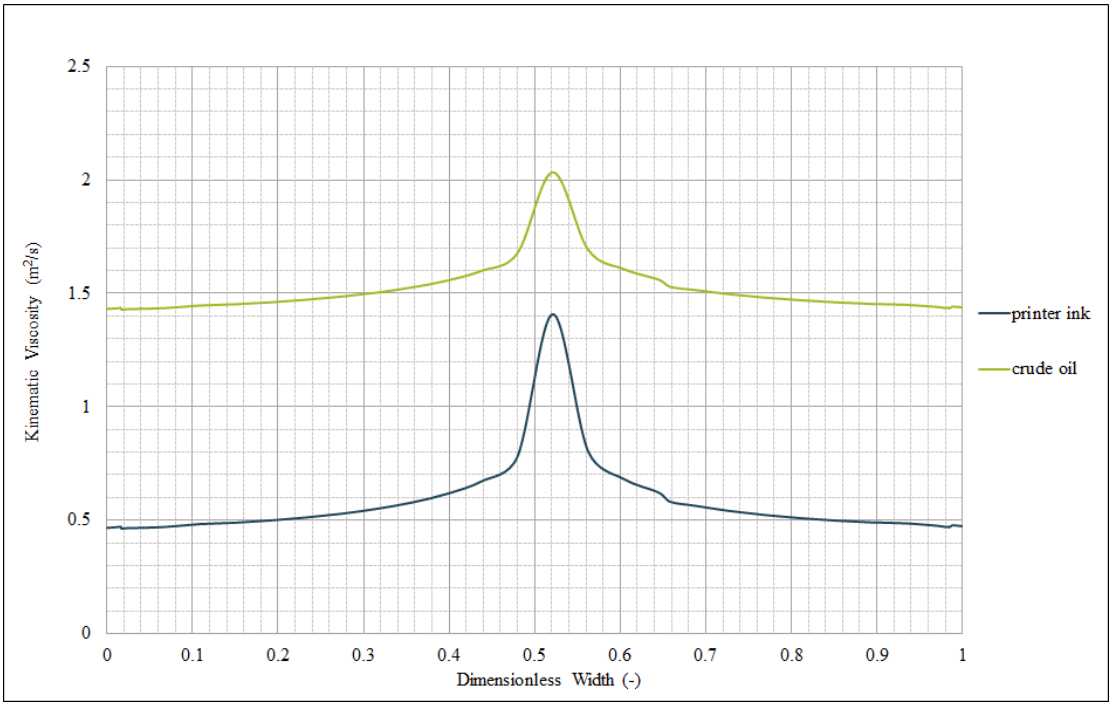

Figure 9b : Kinematic Viscosity at 'x = 7.5 mm' vs Dimensionless Width for Velocity = 0.5 m/s

7. Conclusion :

The fluid consistency index (K) governs the non-Newtonian fluid's intrinsic resistance to deformation under shear. Understanding the influence of K on pressure drop characteristics within the sinusoidal microchannel is vital for engineering applications where non-Newtonian fluids are encountered. For K > 1, pressure variation was considerably higher due to the nonlinear behaviour of power-law fluids. In contrast, Newtonian water displayed minimal pressure variation, confirming its constant viscosity. Additionally, fluid velocity and pressure gradient exhibited a direct relationship, following fluid mechanics principles. The velocity profile at the exit plane showed some interesting characteristics for Xanthan, a non-Newtonian fluid. These findings provide valuable insights into fluid dynamics in complex microgeometries and have important implications for engineering applications involving microchannels and non-Newtonian fluids.

8. Nomenclature

$A -$ Amplitude of wavy wall, m

$K -$ Flow consistency index, Pa. s^n

$L -$ length of channel $(= 100W)$, m

$n -$ flow behavior index

$p -$ pressure, Nm^{-2}

$Re -$ Reynolds number

$Re_{PL} -$ Reynolds number of Power Law Fluid

$v -$ velocity, m/s

$W -$ half width of channel, m

Greek Symbols

$\propto -$ dimensionless amplitude of the sinusoidal wall $(= A/W)$

$\Upsilon -$ wavelength of the sinusoidal wall

$\lambda -$ dimensionless wavelength of the sinusoidal wall $(= \Upsilon/W)$

$\mu -$ dynamic viscosity, kg $m^{-1}s^{-1}$

$\rho -$ Density of fluid, kg/m^3

$\nu -$ kinemactic viscosity, m^2/s

9. References :

Craven, B.A., Faghih, M.M., Aycock, K.I. and Kolahdouz, E.M. (2022). A Poisson equation method for prescribing fully developed non-Newtonian inlet conditions for computational fluid dynamics simulations in models of arbitrary cross-section. *Mathematics and Computers in Simulation, [online]* 194, pp.523–538.

Edwards, M.F., Nellist, D.A., & Wilkinson, W.L. (1972). Unsteady, laminar flows of non-Newtonian fluids in pipes. *Chemical Engineering Science*, 27(2), 295-306.

Fu, T., Carrier, O., Funfschilling, D., Ma, Y. and Li, H.Z. (2016). Newtonian and Non-Newtonian Flows in Microchannels: Inline Rheological Characterization. *Chemical Engineering & Technology*, 39(5), pp.987–992.

Gorthi, S.R., Sanjaya Kumar Meher, Biswas, G. and Pranab Kumar Mondal (2020). Capillary imbibition of non-Newtonian fluids in a microfluidic channel: analysis and experiments. *Proc. R. Soc. A*. 476(2242)

Keslerová, R. (2023). Numerical modelling of generalized Newtonian fluids flow in S-type geometry of bypass. 429, pp.115237–115237.

Koh, Y.H., Ong, N.S., Chen, X.Y., Lam, Y.C. and Chai, J.C. (2004). Effect of Temperature and Inlet Velocity on The Flow of a Nonnewtonian Fluid. *International Communications in Heat and Mass Transfer*, 31(7), pp.1005–1013.

Metzner, A.B. and Reed, J.C. (1955). Flow of non-newtonian fluids—correlation of the laminar, transition, and turbulent-flow regions. *AIChE Journal*, 1(4), pp.434–440.

Mondal, B., Mehta, S.K., Patowari, P.K. and Pati, S. (2019). Numerical study of mixing in wavy micromixers: comparison between raccoon and serpentine mixer. *Chemical Engineering and Processing - Process Intensification*, 136, 44–61.

Nguyen Q-H and Nguye N-D (2012). Incompressible Non-Newtonian Fluid Flows. *Continuum Mechanics - Progress in Fundamentals and Engineering Applications.*

Peng, J.; Huang, J.; Wang, J. Modelling of Power-Law Fluid Flow Inside a Piezoelectric Inkjet Printhead. *Sensors* 2021, *21*, 2441.

Philippou, M., Kountouriotis, Z. and Georgiou, G.C. (2016). Viscoelastic flow development in tubes and channels with wall slip. *Journal of Non-Newtonian Fluid Mechanics, [online]* 234, pp.69–81.

Roumpea, E., Chinaud, M. and Angeli, P. (2017). Experimental investigations of non-Newtonian/Newtonian liquid-liquid flows in microchannels. *AIChE Journal*, 63(8), pp.3599–3609.

Sami, N.A., Ibrahim, D.S. and Abdulrazaq, A.A. (2017). Investigation of non-Newtonian flow characterization and rheology of heavy crude oil. *Petroleum Science and Technology*, 35(9), pp.856–862.